NANO LETTERS

2008
Vol. 8, No. 11
3750-3754

Nanoporous Si as an Efficient Thermoelectric Material

Joo-Hyoung Lee,[†] Giulia A. Galli,[‡] and Jeffrey C. Grossman*[,†]

Berkeley Nanosciences and Nanoengineering Institute, University of California, Berkeley, California 94720, and Department of Chemistry, University of California, Davis, California 95616

Received July 10, 2008; Revised Manuscript Received October 6, 2008

ABSTRACT

Room-temperature thermoelectric properties of n-type crystalline Si with periodically arranged nanometer-sized pores are computed using a combination of classical molecular dynamics for lattice thermal conductivity and ab initio density functional theory for electrical conductivity, Seebeck coefficient, and electronic contribution to the thermal conductivity. The electrical conductivity is found to decrease by a factor of 2−4, depending on doping levels, compared to that of bulk due to confinement. The Seebeck coefficient *S* yields a 2-fold increase for carrier concentrations less than 2×10^{19} cm^{-3}, above which *S* remains closer to the bulk value. Combining these results with our calculations of lattice thermal conductivity, we predict the figure of merit ZT to increase by 2 orders of magnitude over that of bulk. This enhancement is due to the combination of the nanometer size of pores which greatly reduces the thermal conductivity and the ordered arrangement of pores which allows for only a moderate reduction in the power factor. We find that while alignment of pores is necessary to preserve power factor values comparable to those of bulk Si, a symmetric arrangement is not required. These findings indicate that nanoporous semiconductors with aligned pores may be highly attractive materials for thermoelectric applications.

As the world's demand for energy rapidly increases while fossil fuel supplies decrease, it is becoming more important to develop new, inexpensive materials that can supply sustainable and clean energy to meet the needs of the future. One promising approach relies on thermoelectric (TE) materials, which interconvert temperature gradients and electricity on a solid-state basis and thus provide a method of cooling and power generation without refrigerant or moving parts. However, a large increase in the efficiency of current TE materials is needed in order for this energy conversion method to become an abundant resource.

Thermoelectric efficiency is described by the so-called thermoelectric figure of merit $ZT = S^2\sigma T/\kappa$, where T is the absolute temperature, S the Seebeck coefficient, σ the electrical conductivity, and κ the total thermal conductivity, respectively. κ is given as the sum of electrical (κ_e) and lattice (κ_l) contributions. In order for TE materials to become competitive with conventional refrigerators or power generators, they must possess a figure of merit of at least 3.[1] Yet, only $ZT \sim 1$ in bulk materials at room temperature has been achieved since the time when semiconductors were found to be able to act as heat pumps nearly 50 years ago.[1] The central difficulty in increasing ZT lies in the interdependence among S, σ, and κ, in that optimizing one often adversely affects others, which has so far yielded limited applications of TE materials (e.g., radioisotope thermoelectric generators for spacecrafts[2]).

Recent advances in nanostructured semiconductor synthesis, however, have provided a new strategy to this important problem.[3−5] Venkatasubramanian et al. demonstrated[3] that Bi_2Te_3/Sb_2Te_3 superlattices show a large enhancement in ZT up to ~2.4 at room temperature when p-doped, and that $ZT \sim 1.4$ is obtained in n-type $Bi_2Te_3/Bi_2Te_{2.83}Sb_{0.17}$ superlattices. Harman et al.[4] used n-type PbSeTe/PbTe-based quantum dot superlattice structures to achieve $ZT \sim 1.3-1.6$ at room temperature. Androulakis et al.[5] also reported that $ZT \sim 1.45$ is obtained at 630 K in p-type $Ag(Pb_{1-y}Sn_y)_m SbTe_{2+m}$ nanocomposites. We note that the enhancement of ZT in these nanostructures is mainly due to the large reduction of κ_l, arising from phonon scattering in lower dimensions, without changing much the electronic transport, as opposed to an increase in the electronic density of states at the Fermi level which leads to an increase in σ.[6] Although the observed high ZT values in these systems make them attractive for practical TE applications, it may be highly challenging and expensive to fabricate materials such as Bi, Te, Sb, Pb, and Ag into synthetic nanostructures for large-scale energy conversion purposes.[7]

In contrast, Si is the most widely used material in the semiconductor industry with a low-cost and high-yield processing capability. While Si has long been considered to be a very inefficient TE material with $ZT \sim 0.01$ because of its high κ, recent experiments demonstrated a dramatic

* Corresponding author, jgrossman@berkeley.edu.
[†] University of California, Berkeley.
[‡] University of California, Davis.

10.1021/nl802045f CCC: $40.75 © 2008 American Chemical Society
Published on Web 10/24/2008

increase in ZT for Si nanowires (SiNWs). Hochbaum et al. reported the electrochemical synthesis of large-area, wafer-scale arrays of SiNWs with 20−300 nm in diameter.[7] The measured ZT in these nanowires is remarkably high, up to 0.6 at room temperature for 50 nm diameter wires, which is attributed to a 2 orders of magnitude decrease in κ due to the high surface roughness. Boukai et al. also used SiNWs with cross-sectional areas of 10 nm × 10 nm and 20 nm × 20 nm to obtain an approximately 100-fold improvement in ZT over bulk Si over a wide temperature range from 100 up to 350 K,[8] including ZT ∼ 1 at 200 K. The authors ascribed the sharp increase in ZT to the reduction in κ and the phonon drag effect, the latter of which has been known to be small or negligible in previously studied TE materials.[9] These experiments thus open a new pathway into Si-based TE applications, and provide strong motivation to search for other types of Si nanostructures with similarly large values of ZT.

Porous Si generated large interest in the 1990s due to its photoluminescence properties.[10,11] While subsequent research mainly focused on the optoelectronic applications of porous Si, several experiments[12,13] revealed extremely low κ in this structure, suggesting the possibility of its TE applications. Thermal conductivity of porous Si with the volume fraction of pores ranging from 0.64 to 0.89 is found to be as low as 0.1 W/mK for randomly distributed pores at room temperature, 3 orders of magnitude smaller than that of the bulk.[12] Although these observations are encouraging, the electronic structure of this "traditional" porous Si is also substantially deteriorated due to the randomness of pore arrangement and shapes, which results in very low electrical conductivity (σ ∼ 0.2 S/cm) and consequently figure of merit (ZT ∼ 0.03) at room temperature.[13] On the other hand, if the pores were ordered instead of random, one would expect a significant improvement in the electrical conducvitivity with respect to the randomly distributed cases. Measurements of the in-plane κ of Si films with periodically arranged *micrometer-sized* pores were reported to yield κ as low as 40 W/mK at room temperature.[14] While this value is large compared to that of randomly distributed porous Si, recent molecular dynamics (MD) studies predicted that in-plane $\kappa_l \sim 0.6$ W/mK could be achieved with ordered *nanometer-sized* pores (nanoporous Si, npSi) due to the increased phonon−phonon and phonon−surface scattering,[15] despite the periodic arrangement of pores.

Here, we perform room-temperature transport calculations for n-type nanoporous Si as a function of pore size (d_p) and spacing (d_s) using ab initio electronic structure calculations and the Boltzmann transport approach. Our results show that σ and κ_e in these systems are reduced by at least a factor of 2 from the corresponding bulk values due to the in-plane confinement, whereas S increases from that of bulk for low carrier concentrations. Combined with our MD calculations for κ_l, including previous results[15] and new calculations to investigate pore shape dependence, we predict ZT to be as high as 0.4. These findings make ordered npSi highly attractive for possible TE cooling applications and point toward an alternative approach for employing nanostructured semiconductors as efficient TE materials which may have advantages over the nanowire systems.

Transport coefficients are calculated by defining the following function within the constant relaxation time approximation[16]

$$\mathbf{L}^{(\alpha)} = e^2\tau\sum_n \int \frac{\mathbf{dk}}{4\pi^3}\left(-\frac{\partial f(\epsilon_{n\mathbf{k}})}{\partial \epsilon_{n\mathbf{k}}}\right)\mathbf{v}_{n\mathbf{k}}\mathbf{v}_{n\mathbf{k}}(\epsilon_{n\mathbf{k}}-\mu)^{\alpha} \qquad (1)$$

in terms of which $\sum = \mathbf{L}^{(0)}$, $\mathbf{S} = -(1/eT)\sum^{-1}\mathbf{L}^{(1)}$, and $\mathbf{K} = (1/e^2T)(\mathbf{L}^{(2)} - \mathbf{L}^{(1)}\sum^{-1}\mathbf{L}^{(1)})$ are evaluated, and the electrical conductivity, Seebeck coefficient, and electronic thermal conductivity are obtained through $\sigma = (\sum_{xx} + \sum_{yy})/2$, $S = (\mathbf{S}_{xx} + \mathbf{S}_{yy})/2$, and $\kappa_e = (K_{xx} + K_{yy})/2$ due to the planar symmetry of the present geometry. Here, $\epsilon_{n\mathbf{k}}$ is the energy eigenvalue in the nth band at $\mathbf{k}$, $f(\epsilon_{n\mathbf{k}})$ the Fermi−Dirac function at temperature T, μ the chemical potential, τ the relaxation time, and $\mathbf{v}_{n\mathbf{k}} = (1/\hbar)\nabla_{\mathbf{k}}\epsilon_{n\mathbf{k}}$, respectively. Note that τ is taken to be energy-independent, although given as a function of the carrier concentration, which is obtained by fitting experimental values for bulk Si.[17]

The relaxation time in semiconductors is determined mainly by impurity scattering and the acoustic and optical deformation potential scattering.[18] Unlike a one-dimensional nanowire or two-dimensional quantum well structure, ordered npSi is a topologically connected and three-dimensional structure, so the bulk expression for τ is expected to be a reasonable approximation. For impurity scattering, τ is inversely proportional to the concentration of impurities (N_I) in the crystal. Since N_I is the same for both bulk and npSi for a uniform distribution of impurities in both systems, the impurity contribution to τ is expected to be largely unaffected by pores. For scattering contributions from electron−phonon interactions, if we assume the deformation potential to be the same for npSi as in bulk, the contribution from the acoustic deformation potential scattering remains unchanged for npSi because the number of acoustic branches in the phonon dispersion to which $1/\tau$ is proportional is the same with and without pores. On the other hand, the number of dominant optical phonon branches for scattering is generally reduced for npSi compared to the bulk, which leads to an increase in τ over the bulk value. A recent study[19] showed that τ of SiNWs, obtained from bulk mobility data, yields reasonable agreement with a more detailed calculation using the scattering matrix elements, which reveals an increase in τ by a factor of 1−4 compared to that of bulk for boron-doped wires. In this work, we use the bulk value for τ, which will thus serve to provide lower bounds for transport coefficients such as σ and κ_e. Note that in the constant relaxation time approximation, the Seebeck coefficient S is independent of τ since S is proportional to $\mathbf{L}^{(0)-1}\mathbf{L}^{(1)}$ (eq 1), and the electronic part of the thermal conductivity, which appears in the denominator of the figure of merit ZT, depends only linearly on τ.

Figure 1 shows the structure of npSi used in our calculations for circular and square pores. In-plane transport coefficients (S, σ, and κ_e) are calculated for two different cases: (1) d_s is varied, keeping d_p fixed at 1.0 nm and (2) d_p is varied while d_s is fixed at 1.0 nm. With the pores aligned along the z-axis, a supercell is composed of three (four)

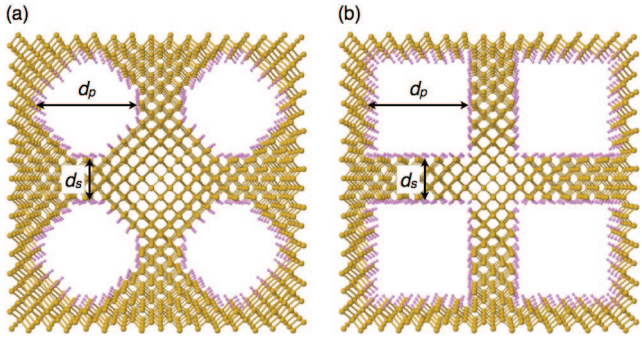

Figure 1. Structure of nanoporous Si (orange) passivated with H (purple) atoms along with structural variables used in the calculations: (a) circular and (b) square pores. Pores are along the [001] direction.

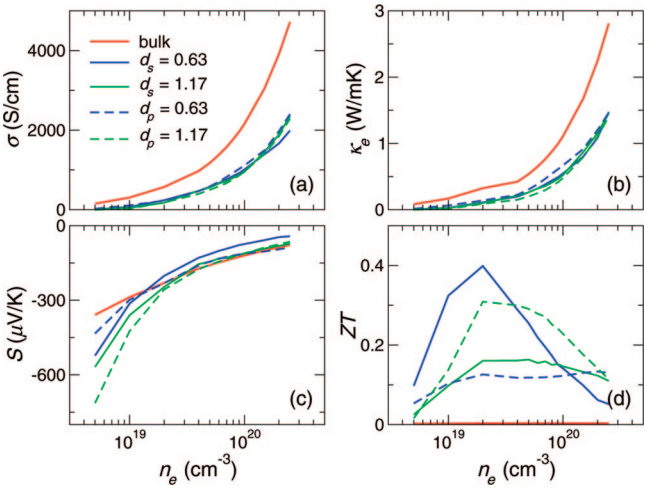

Figure 2. Room-temperature transport coefficients of ordered nanoporous Si with circular pores: (a) electrical conductivity, (b) electronic thermal conductivity, (c) Seebeck coefficient, and (d) figure of merit. Solid curves are for fixed d_p cases, and dotted ones for fixed d_s cases, respectively. Bulk values are presented for comparison.

conventional cells in the *xy*-plane for smaller (larger) $d_s(d_p)$ values in fixed $d_p(d_s)$ cases, respectively.

The coefficients are calculated as a function of carrier concentration (described by a Fermi function within the range $10^{19}-10^{20}$/cm^3) within a fixed band approximation in order to find the optimal doping range for TE applications. All electronic structure calculations are performed within the density functional theory approach[20,21] as implemented in the Vienna Ab Initio Simulation Package,[22] using a 26 Ry plane-wave cutoff, ultrasoft Vanderbilt-type pseudopotentials,[23,24] and the generalized gradient approximation[25] of Perdew and Wang for exchange correlation energy. In addition, a dense **k**-point mesh is used containing 150 points in the irreducible Brillouin zone despite the large supercells, which is necessary to obtain converged results for the transport coefficients.

Our calculated σ, κ_e, S, and ZT as a function of doping concentration (n_e) at room temperature are presented in Figure 2 for circular pores. As is seen from Figures 2a,b, σ and κ_e increase with n_e as more carriers contribute to the transport. Clearly, the presence of pores reduces σ and κ_e compared to bulk; however, the reduction is much less

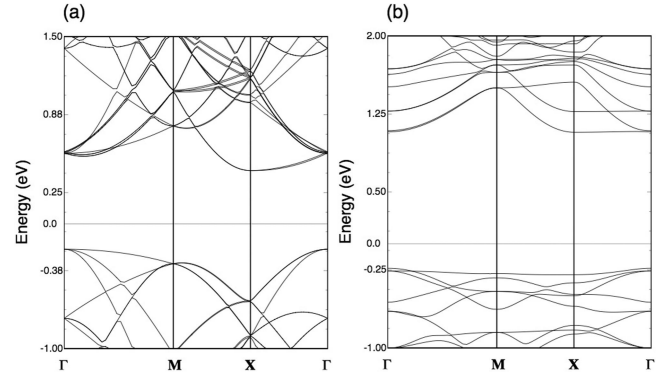

Figure 3. Band structure of Si: (a) bulk and (b) nanoporous with $(d_p, d_s) = (1.0, 0.63)$ nm. In both cases, the same tetragonal symmetry was used to facilitate comparison.

significant than that observed in κ_l. κ_l shows more than a 200-fold reduction from the bulk value,[15] whereas σ and κ_e are reduced by a factor of 2−4 depending on the carrier concentration. This is in sharp contrast to traditional porous Si with randomly distributed pores, for which σ is reduced from the bulk value by several orders of magnitude.[13]

The band structure of circular pores, shown in Figure 3, shows that introducing ordered nanopores removes most degeneracies at high symmetry points in the band structure of the bulk and increases the band gap: the calculated band gap is 0.61 eV for bulk, whereas it ranges from 0.90 to 1.36 eV in our npSi depending on the values of d_p and d_s. Furthermore, pores induce band flattening along the $\Gamma \rightarrow X$ direction due to the confinement,[26] which results in a reduction of σ and κ_e. However, the band structure along other directions such as $\Gamma \rightarrow M$ and $M \rightarrow X$ of npSi remains as dispersive as that in the bulk, and the reduction in σ and κ_e is not nearly as significant as in κ_l. We note that while the electronic structure of a particular case with $(d_p, d_s) = (1.0, 0.63)$ nm is discussed above, geometries with different (d_p, d_s) values yield similar flattening and dispersiveness near the conduction band minimum (CBM). This leads to the similarities in the electronic transport properties of different pore structures as shown in Figure 2.

It is interesting to observe the difference and similarity in the behavior of S as a function of n_e between npSi and bulk (Figure 2c). Since S is proportional to the ratio of σ'/σ (where σ' is the derivative of σ with respect to energy, computed at the Fermi level, E_F), for similar variation of the conductivity close to the Fermi level, S is expected to increase as σ decreases in going from the bulk to npSi. This is indeed the case for $n_e < 2 \times 10^{19}$ cm^{-3}. However, for $n_e \geq 2 \times 10^{19}$ cm^{-3}, E_F lies deep inside the conduction band for both npSi and bulk, where single particle energies are symmetrically distributed around E_F. Since E_F is found to be higher in energy from the CBM for npSi than in the bulk case for $n_e \geq 2 \times 10^{19}$ cm^{-3}, it is not surprising that the corresponding $|S|$ values of npSi become smaller than the bulk values. It is also worth noting that the σ and $|S|$ values in the present work are in the same range as those computed previously for SiNWs with dimensions similar to our pore size and spacing.[19] However, although the npSi system is in a sense

Table 1. Lattice Thermal Conductivity of Nanoporous Si with Circular (κ_l^C) and Square (κ_l^S) Pores, Respectively, For Different d_p and d_s.

fixed (nm)	d_s (nm)	d_p (nm)	κ_l^C (W/mK)	κ_l^S (W/mK)
d_p=1.0	0.63		0.6 ± 0.1	0.6 ± 0.1
	1.17		1.9 ± 0.2	2.5 ± 0.2
d_s=1.0		0.63	2.8 ± 0.2	0.9 ± 0.1
		1.17	1.1 ± 0.1	1.2 ± 0.1

the "inverse" of the SiNW, a direct comparison is not possible since in the nanowire case transport properties are calculated along the wire axis while for npSi we compute properties perpendicular to the pore axis.

Calculated ZT values are presented in Figure 2d. Clearly, ZT of npSi is significantly increased compared to that of bulk Si: our calculations for the bulk give ZT $\sim$ 0.003 in the entire carrier concentration of interest, whereas the corresponding values of npSi are predicted to be as large as to 0.4 at $n_e = 2 \times 10^{19}$ cm^{-3}. Because the power factor decreases for npSi by more than 30% from bulk values, the enhancement in ZT by 2 orders of magnitude is due to the large reduction in κ_l for the porous structure. We note that κ_l and κ_e are of the same order of magnitude in npSi and κ_e is always smaller than the corresponding values in the bulk.

We also carried out a similar set of calculations for pores with square shapes, as shown in Figure 1b. In order to examine the dependence of both electrical and thermal transport properties on pore shape, the lattice thermal conductivities for square pores (κ_l^S) are calculated with the same classical MD approach used in ref 15; the results are listed in Table 1 along with those for circular pores (κ_l^C) for comparison. While κ_l^S remains close to κ_l^C in most cases, it is reduced by a factor of 3 for (d_p, d_s) = (0.63, 1.0) nm. We postulate that this reduction originates from a different passivation at the pore surface: for this particular pore size and spacing, in circular pores all Si atoms have a single H-bond at the surface, whereas Si is bound to two hydrogens at the surface of square pores. The increase in the number of Si−H at the pore surfaces for the square pores enhances to some extent surface roughness and thus may reduce the lattice thermal conductivity due to increased phonon surface scattering; however, additional work is needed to further explore this interpretation. On the other hand, all the electronic transport coefficients (σ, κ_e, and S) remain similar to those of Si with circular pores, which implies that varying the pore shape does not have a sizable effect on the TE properties of npSi except for the (d_p, d_s) = (0.63, 1.0) nm case as discussed above.

The results thus far are for pores that are aligned *and* arranged in a perfectly symmetric, ordered structure; however, in realistic materials, depending on the synthesis approach, it may be challenging to control the pore arrangement to such a high degree of order. Thus, it is important to examine the effect of having asymmetric configurations of pores on the thermoelectric properties. As it was already shown that the presence of asymmetric pore arrangements would not change in a significant manner the lattice thermal conductivity,[15] we focus here on the effect of asymmetric pores on the electronic transport. To this end, a supercell

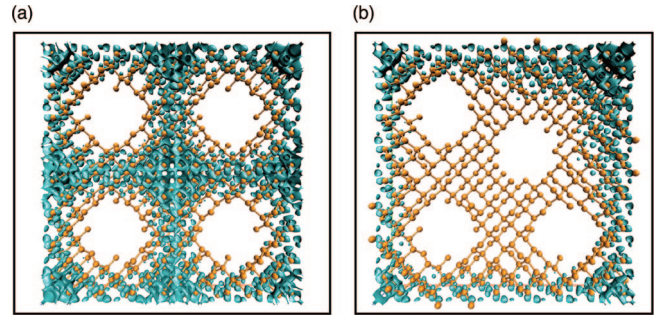

Figure 4. Constant density surfaces (40% of the maximum values) are shown for (a) $\delta = 0$ and (b) $\delta = 0.15$. H atoms on the pore surfaces are not shown for visibility.

containing four pores is considered with one of them displaced from its equilibrium position by $a_{latt}(\delta, \delta, 0)$ where a_{latt} is the lattice constant (see Figure 4); electronic structure calculations are performed for δ increasing from 0 (ordered) to 0.175 (corresponding to a 1.08 nm displacement of the pore center from its ordered position). As δ increases, we observe a flattening in the conduction band along high symmetry lines. For example, the energy differences $\Delta E(\Gamma - M)$ and $\Delta E(M - X)$ gradually decrease as δ increases up to a displacement of the pore by $\sim$0.46 nm, beyond which the flattening of the bands becomes much more substantial and ΔE drops considerably. Figure 4 shows the sum of the square moduli of the electronic states within 0.1 eV energy interval from the CBM for two separate pore displacements. In the ordered case ($\delta = 0$), the states are delocalized and conduction channels are present throughout the entire system. Although for $\delta \neq 0$, there is a decrease in charge density in the regions in between the displaced pore, there are still states delocalized over the entire system. This indicates that most likely a perfect symmetric arrangement of pores is *not* required to maintain good electronic conduction properties.

It should be noted that for bulk Si, our computed ZT values are underestimated by a factor of 3 compared to experiment. In our MD calculations, the use of a Tersoff potential tends to overestimate κ_l, possibly by a factor of 2. In addition, the computational approach employed in the present work is expected to overesitmate σ approximately by the same factor compared to experiment,[27] whereas $|S|$ is likely to be underestimated by nearly 40%, which leads to a $\sim$25% decrease in the power factor and thus results in the observed discrepancy in ZT. While we cannot state quantitatively that the same underestimate holds for npSi, for the reasons discussed above it is nonethless likely that our predicted value of ZT $\sim$ 0.4 for npSi is an underestimate by a factor of 2−3.

It is worthwhile to compare the present results with those of SiNWs which were recently reported.[7,8] While ZT values of npSi may be similar to those of wires with comparable diameter,[19] npSi may provide a few potential advantages over the NW cases. From a manufacturing point of view, ordered npSi may be realized from the bulk material for which well-established growing techniques such as the Czochralski process[28] exist. After fabricating Si-wafers from bulk, patterns of aligned pores could be generated using a range

of synthesis approaches, e.g., ion lithography,[29,30] etching,[31] irradiation with fullerenes,[32] or surfactant-driven self-assembly.[33,34] It would also be relatively straightforward to connect npSi to electrical leads due to its bulk nature, which is necessary to make TE modules for applications. This is in contrast with the challenge associated with keeping good contact between an array of SiNWs and electrical leads. Furthermore, synthesizing npSi from a bulk host provides a simple way of doping in that once the bulk is doped with a desired carrier concentration, npSi will naturally inherit essentially the same doping level. Finally, we note that besides optimizing TE properties by varying pore size and spacing, it may be possible to tune the electronic transport properties of npSi by filling the pores with appropriate materials. For example, pores can be filled either partly or fully to form a nanocomposite to tailor the electronic properties for further optimization of the figure of merit without increasing the lattice thermal conductivity. These features along with the high ZT values make ordered npSi highly appealing for TE cooling applications.

Acknowledgment. This work was performed under the auspices of the National Science Foundation by University of California Berkeley under grant no. 0425914 and the Defense Advanced Research Projects Agency under grant no. W911NF-06-1-0175. Computations were performed at the National Energy Research Scientific Computing Center.

References

(1) Majumdar, A. *Science* **2004**, *303*, 777.
(2) Yang, J.; Caillat, T. *MRS Bull.* **2006**, *31*, 224.
(3) Venkatasubramanian, R.; Siivola, E.; Colpitts, T.; O'Quinn, B. *Nature* **2001**, *413*, 597.
(4) Harman, T. C.; Taylor, P. J.; Walsh, M. P.; LaForge, B. E. *Science* **2002**, *297*, 2229.
(5) Androulakis, J.; Hsu, K. F.; Pcionek, R.; Kong, H.; Uher, C.; D'Angelo, J. J.; Downey, A.; Hogan, T.; Kanatzidis, M. G. *Adv. Mater.* **2006**, *18*, 1170.
(6) Tritt, T. M.; Subramanian, M. A. *MRS Bull.* **2006**, *31*, 188.
(7) Hochbaum, A. I.; Chen, R.; Delgado, R. D.; Liang, W.; Garnett, E. C.; Najarian, M.; Majumdar, A.; Yang, P. *Nature* **2008**, *451*, 163.
(8) Boukai, A. I.; Bunimovich, Y.; Tahir-Kehli, J.; Heath, J. R. *Nature* **2008**, *451*, 168.
(9) Vining, C. B. *Nature* **2008**, *451*, 132.
(10) Canham, L. T.; Leong, W. Y.; Beale, M. I. J.; Cox, T. I.; Taylor, L. *Appl. Phys. Lett.* **1992**, *61*, 2563.
(11) Cullis, A. G.; Canham, L. T.; Calcott, P. D. J. *J. Appl. Phys.* **1997**, *82*, 909.
(12) Gesele, G.; Linsmeier, J.; Drach, V.; Fricke, J.; Arens-Fischer, R. *J. Phys. D* **1997**, *30*, 2911.
(13) Yamamoto, A.; Takazawa, H.; Ohta, T. *Proc. Int. Conf. Thermoelectr.* **1999**, 428.
(14) Song, D.; Chen, G. *Appl. Phys. Lett.* **2004**, *84*, 687.
(15) Lee, J.-H.; Grossman, J. C.; Reed, J.; Galli, G. *Appl. Phys. Lett.* **2007**, *91*, 223110.
(16) Ashcroft, N. W.; Mermin, N. D. *Solid State Phys.*; Saunders College Publishing, 1976.
(17) Gaymann, A.; Geserich, H. P.; v. Löhneysen, H. *Phys. Rev. B* **1995**, *52*, 16486.
(18) Seeger, K. *Semiconductor Physics: An Introduction*, 9th ed.; Springer: Berlin, 2004.
(19) Vo, T. T. M.; Williamson, A. J.; Galli, G. A. *Nano Lett.* **2008**, *8*, 1111.
(20) Hohenberg, P.; Kohn, W. *Phys. Rev.* **1964**, *136*, B864.
(21) Kohn, W.; Sham, L. J. *Phys. Rev.* **1965**, *146*, A1133.
(22) Kresse, G.; Furthmueller, J. *Phys. Rev. B* **1996**, *54*, 11169.
(23) Vanderbilt, D. *Phys. Rev. B* **1990**, *41*, 7892.
(24) Kresse, G.; Hafner, J. *J. Phys.: Condens. Matter* **1994**, *6*, 8245.
(25) Perdew, J. P.; Wang, Y. *Phys. Rev. B* **1992**, *45*, 13244.
(26) Mingo, N.; Broido, D. A. *J. Appl. Phys.* **2007**, *101*, 014322.
(27) Weber, L.; Gmelin, E. *Appl. Phys. A: Mater. Sci. Process.* **1991**, *53*, 136.
(28) Yu, P. Y.; Cardona, M. *Fundamentals of Semiconductors*, 3rd ed.; Springer: Berlin, 2001.
(29) Razpet, A.; Johansson, A.; Possnert, G.; Skupíski, M.; Hjort, K.; Hallén, A. *J. Appl. Phys.* **2005**, *97*, 044310.
(30) Bianconi, M.; Bergamini, F.; Cristiani, S.; Lulli, G. *J. Appl. Phys.* **2007**, *102*, 074307.
(31) Striemer, C. C.; Gaborski, T. R.; McGrath, J. L.; Fauchet, P. M. *Nature* **2007**, *445*, 749.
(32) Dunlop, A.; Jaskierowicza, G.; Della-Negrab, S. *Nucl. Instrum. Methods, B* **1998**, *146*, 302.
(33) Armatas, G. S.; Kanatzidis, M. G. *Science* **2006**, *313*, 817.
(34) Sun, D.; Riley, A. E.; Cadby, A. J.; Richman, E. K.; Korlann, S. D.; Tolbert, S. H. *Nature* **2006**, *441*, 1126.

NL802045F